Structures 59 (2024) 105690

Contents lists available at ScienceDirect

Structures

journal homepage: www.elsevier.com/locate/structures

Bending resistance of austenitic stainless steel hollow sections at elevated temperatures

Paulo A.G. Piloto [a,*], Luís M.R. Mesquita [b], Áureo A.T. Cruz [a], Nuno Lopes [c], Flávio Arrais [c], Paulo Vila Real [c]

[a] LAETA-INEGI, Instituto Politécnico de Bragança, Portugal
[b] ISISE, Instituto Politécnico de Bragança, Portugal
[c] RISCO, Department of Civil Engineering, University of Aveiro, Portugal

ARTICLE INFO

Keywords:
Stainless steel beams
Fire
Elevated temperatures
Bending resistance
Experimental investigation
Numerical investigation

ABSTRACT

The present research aims to increase the knowledge of the structural behaviour of stainless steel members under fire. Eight experimental bending tests at elevated temperatures (500, 700 ºC) built with RHS 150×100×3 austenitic stainless-steel beams, using two different grades (1.4301, 1.4571) also known as 304 and 316Ti, are presented. Both grades 1.4301 (X5CrNi18–10) and 1.4571 (X6CrNiMo17–12–2) have almost the same core chemical composition but there are some differences, especially the grade 1.4571 has 2–2.5% molybdenum and a small amount of titanium (less than 0.7%). Grade 1.4301 presents good rust resistance, sufficient acid resistance and good weldability, while grade 1.4571 presents very good rust resistance, very good acid resistance and also good weldability. Both have almost the same strength, but grade 1.4571 has superior strength at elevated temperatures. Both material grades were experimentally characterised with coupon tensile tests at room temperature. The load-displacement behaviour is validated with 3D shell finite element models, assuming a true stress-strain material model, based on the two-stage Ramberg Osgood constitutive law. With the developed numerical model, a parametric analysis is presented to study the fire resistance of beams from both materials, using three different cross-sections and eleven different temperatures. The bending resistance obtained with the finite element model is in good agreement with the cross-sectional design moment resistance, when considering the effective area, confirming that the design rules from EN1993–1–2 are safe for less slender cross-sections and unsafe for the most slender cross-sections.

1. Introduction

The fire behaviour of stainless steel beams has been the subject of different research studies, with both experimental tests and numerical analyses, providing valuable information on the topic. In general, it has been shown that their strength and stiffness retentions at elevated temperatures are significant, which can contribute to the increase of the usage of this material in structural applications.

Rasmussen and Hancock [1] developed a nonlinear method to determine deflections of stainless steel beams, based on secant and tangential modulus of elasticity, validated against experimental results on 4-point bending tests, with reasonable agreement. Gardner and Baddoo [2] presented experimental fire tests on four stainless steel beams, applied to validate a numerical model used afterwards in a parametric analysis. Recommendations were included in reference documents, such as the design manual for structural stainless steel from SCI [3] and implemented in the Eurocode EN1993–1–2 [4], with small adjustments in design rules for similarity with carbon steel. Gardner and Ng [5] compared the physical properties of austenitic stainless steel with the ones of carbon steel, on the prediction of the beam temperature development under standard fire. New thermal parameters were proposed for the convection coefficient heat transfer and the emissivity of stainless steel. The shadow effect has not been included in the computational model as it should be using the average view factors for each protected surface. Instead, these authors proposed to allow the shadow effects indirectly by modifying the finite element results. Ng and Gardner [6] examined previous experimental tests developed on six stainless steel beams by conducting a numerical investigation towards the prediction of their critical temperatures, which resulted in the proposal of improvements on the design rules of the current version of EN1993–1–2

* Correspondence to: Campus Santa Apolónia, 5300-253 Bragança, Portugal.
E-mail address: ppiloto@ipb.pt (P.A.G. Piloto).

https://doi.org/10.1016/j.istruc.2023.105690
Received 13 September 2023; Received in revised form 22 November 2023; Accepted 1 December 2023
Available online 8 December 2023

[4]. These beams have similar slenderness to the ones used in the present investigation. Lopes et al. [7] numerically modelled the behaviour of thin-walled stainless steel members (flexural buckling in SHS columns and lateral-torsional bucking in I-beams) under fire, analysing the influence of initial imperfections such as residual stresses on their bearing capacity. The effect of the residual stress field was found to be small on the ultimate load-bearing capacity of class 1 beam sections. Huang & Young [8] conducted a numerical investigation regarding the behaviour of lean duplex stainless steel beams at elevated temperatures (from 24 to 900 ºC). The results were compared with the design rules to determine the reliability and concluded that, in general, standards are conservative in predicting the bending resistance at elevated temperatures. Xing et al. [9] conducted an experimental investigation on the bending resistance around the weak axis at elevated temperatures (4-point bending tests) and concluded that all specimens presented a considerable inelastic strength reserve. These experimental tests were used to improve the design predictions of the bending resistance using the plastic effective width method. More recently, Lopes et al. [10] made an experimental investigation on austenitic stainless steel beams with grade 1.4301, using hollow cross-section RHS 150×100×5 at elevated temperatures (steady-state tests at 500, 600 and 700) and under standard fire conditions (transient tests). The material was characterised at room and elevated temperatures. Numerical validation with the software SAFIR is also presented and the analytical method used for the steady state conditions predictions provided a good agreement on the load-deflection behaviour.

Other research works on stainless steel members under fire have been focusing on the development of more accurate and safe new design formulae (such as Xing et al. [11], Vila Real et al. [12], Xing et al. [13]), but still, there is lack of experimental evidence of the fire resistance of stainless steel members, in particular on beams, made of the grade 1.4571 at elevated temperatures.

The present study details the results and observations obtained from experimental fire resistance tests on stainless steel 1.4301 and 1.4571 beams (3-point bending test). The constant temperature has been applied previously to the application of the load (steady state condition). Local instability of the web defined the maximum load-bearing capacity. The eight experimental tests performed at 500 ºC and 700 ºC were developed using the same experimental setup presented in previous works [10], but using two different grades 1.4301 and 1.4571, for the same hollow cross-section RHS 150×100×3.

Coupon tests were used to determine the mechanical properties at room temperature. The material properties at elevated temperatures were defined by the reduction coefficients included in the second generation of the EN1993–1–2 [14]. The reduction factors used for grade 1.4571 were found to be much higher than 1.4301 at 700ºC, which is reflected in the over-prediction of the bending resistance during the validation of the experimental tests. This suggests that tensile tests for grade 1.4571 at 700ºC are required in future investigations.

Numerical simulations of the bending tests, based on geometrically and materially nonlinear analysis with imperfections (GMNIA), with 3D shell181 finite element models (ANSYS) were developed, using full integration with incompatible modes. The numerical model also included higher stiffness elements to mimic the loading system, herein represented by the beam188 finite element (ANSYS). The model was able to accurately predict the maximum bending resistance and follow the post-local buckling behaviour of the webs. Two different numerical models were tested to include the strain-hardening effect of the corners. The inclusion of this effect is responsible for overpredicting the bending resistance, especially to grade 1.4571. This fact also justifies the future measurement of the material behaviour in this region in future investigations.

After the numerical model validation, sixty-six simulations were developed, considering the two stainless steel grades, three different cross-sections, and eleven temperature levels, making it possible to better understand the accuracy and safety level of Eurocode fire design rules for stainless steel beams in case of fire.

2. Experimental tests

Experimental tests were performed for material characterisation at room temperature and to determine the bending resistance of hollow stainless steel beams under 3-point bending tests, using steady-state conditions at elevated temperatures (500 ºC and 700 ºC).

2.1. Coupon tensile tests

Tensile tests were performed on the stainless steel coupons at room temperature (three of the grade 1.4301 and four of the grade 1.4571). Coupons were machined from the web and from the flange (not including the welding seam) of the profiles with the hollow cross-section RHS 150×100×3 mm. The standard tensile test was developed according to EN ISO 6892–1 [15], using an incremental displacement of 1.35 mm/min in the very beginning for the determination of the yield stress, which corresponds to a strain rate of 0.00025 [-/s] over the parallel length L_c. This incremental displacement changed to a second speed of 2.70 mm/min after a 5% strain value. Some coupons were extracted from the web and others from the flange, using the dimensions presented in Fig. 1. No material sample was extracted from the corners, where higher strength is expected along with lower ductility [16].

Fig. 2 depicts the comparison of the obtained engineering stress-strain results with the model used for the material behaviour in the simulation, proposed on the second generation of EN1993–1–2 [14]. This curve was then modified to use the true stress and true strain curve at each temperature level.

The average and the standard deviation values, obtained from tensile tests, are presented in Table 1 for both material grades. The reproducibility of the tested coupons is good, allowing for a small standard deviation.

The results include the maximum load during the tests (Fm), the ultimate stress (σ_u), the proportional stress at 0.2% strain ($\sigma_{p0.2}$), the total strain at the proof stress (ε_c), the proportional stress at 0.01%, 0.05% and 1% strain ($\sigma_{p0.01}$,$\sigma_{p0.05}$,$\sigma_{p1.0}$), the total strain at 1% ($\varepsilon_{1.0}$), the stress at 2% total strain ($\sigma_{2.0}$), the strain at maximum stress (ε_u), the correction factor ($k_{2\%}$) to determine the yield strength obtained from the annex C in EN1993–1–2 [4]and the new reduction coefficient defined by the second generation in FprEN1993–1–2 [14], and finally the elastic modulus (E_a) obtained between 0% and 0.1% total strain. The elastic modulus was determined between this interval due to the high non-linearity of the stress-strain curve from the very beginning. These values have been used to build the constitutive law for each stainless steel grade at room temperature and at elevated temperatures. The two-stage model from the Ramberg-Osgood from the current version of the EN1993–1–4 [17] has been used at room temperature, and from the second generation of the EN1993–1–2 [14] at elevated temperature using the corresponding reduction coefficients.

2.2. Bending tests

This experimental investigation is developed with a fire-resistance furnace and a steel portal frame. The reaction frame is responsible for holding the beam and applying the load, using the 3-point bending test configuration. The beam is positioned in the vertical direction and the load is applied by the hydraulic jack in the horizontal direction. The experimental test runs with steady-state heating conditions (constant temperature inside the furnace) and under major axis bending, see Fig. 3.

The temperature of the beam is controlled by 10 thermocouples, two for each position identified from T1 to T3, with an extra set of thermocouples near the internal limits of the heating zone. The temperature of the furnace is controlled by one plate thermocouple (TG=FURNACE). Tests were developed at 500 ºC and 700 ºC for each material grade

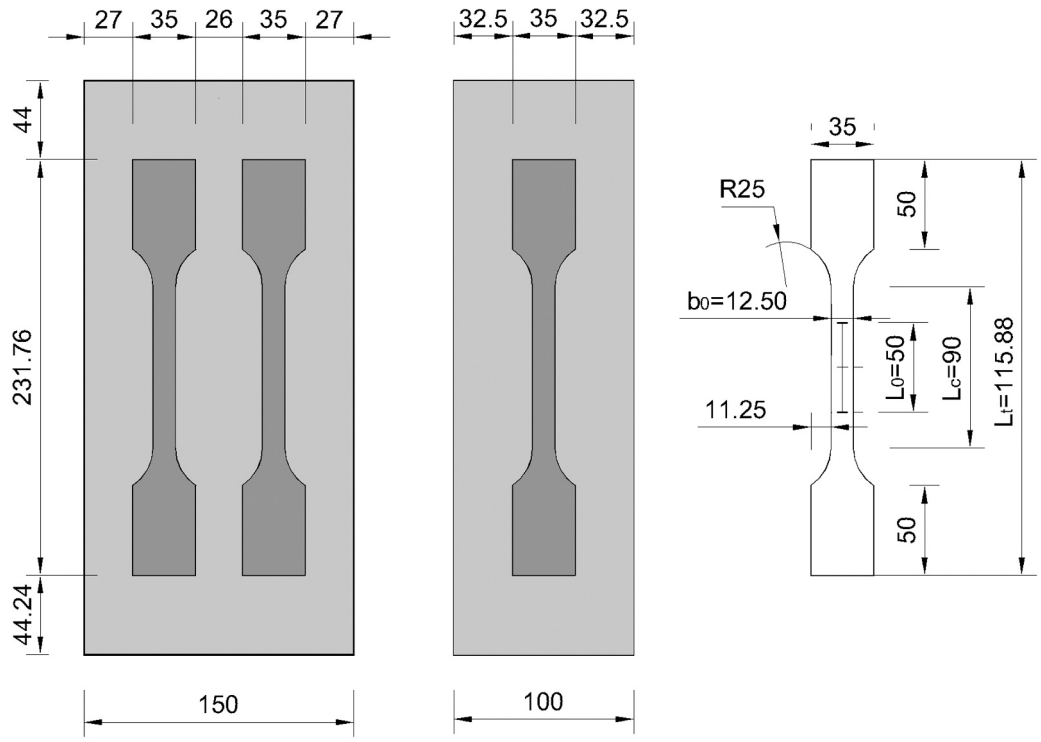

Fig. 1. Coupons dimensions machined from stainless steel profiles.

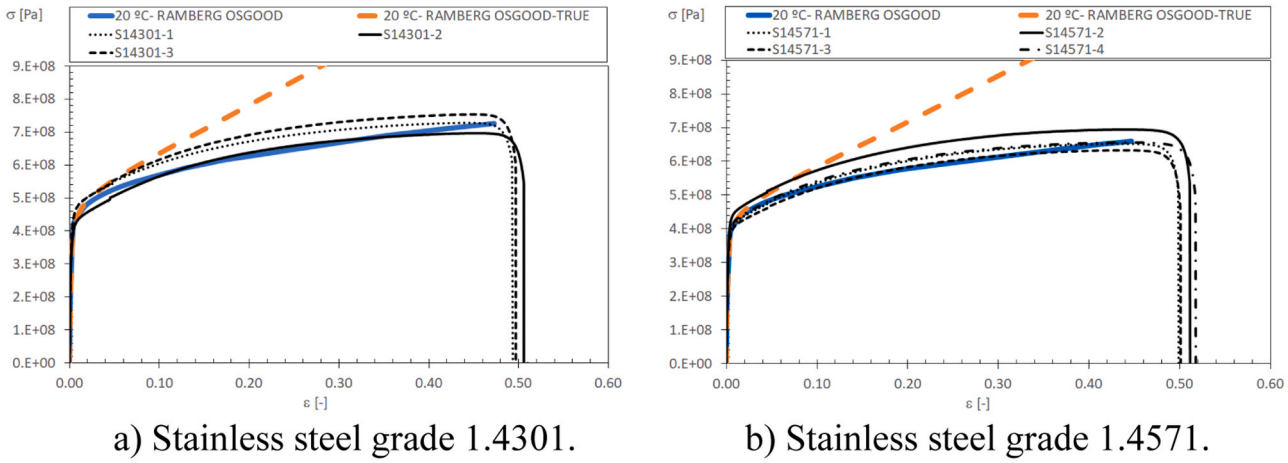

Fig. 2. Stress-strain for both steel grades (Experimental results and material model at room temperature).

(steady state), according to Table 2. The pre-heating phase followed the heating rate defined by ISO834. The adjustment of the load and displacement was made after a long period of temperature stabilisation. The same results would be expected if one had considered a slower or faster heating rate, between 2 and 50 K/min [4].

The temperature evolution is presented for each beam, see Fig. 4. After 20 min, the beams have an almost uniform temperature, when comparing the measurements in the locations T1, T2 and T3. The heating rate follows the standard fire curve, see the furnace temperature evolution (FURNACE). Extra measurements were developed at the bottom and top of the furnace and these temperatures were slightly below the testing temperature, (−11.7% on average for all the specimens), due to the heat loss from the bottom and top of the furnace (conduction through the stainless steel beam, even using internal insulation in the cross-section in these regions).

The heating process was kept without loading conditions for approximately 40–53 min (depending on the specimen, to make sure that the temperature was stable and uniform inside the furnace) and then, the load was increased over time to determine the bending resistance.

The load-displacement results are presented in Fig. 5 for each specimen. The analytical results proposed by EN1993–1–4 [17] and by Rasmussen et al. [1] are included (see Section 3) and the numerical results are also superposed (see Section 4).

The top support was made with a vertical steel part connected to the reaction frame by an endplate, see Fig. 6.

The deformed shape mode for all the specimens is shown in Fig. 7. Here one can see the local deformation on all the test specimens and the heat-affected zones. Also, the colour changes with the temperature level, where thermal oxides are developed on the exposed surface. Stainless steel colours are usually produced at a temperature level over a range from 300 to 850 ºC, and the colour developed depends on the time

Table 1
Average values from tensile tests at room temperature (engineering data).

Property	Units	Average 1.4301	Sd. Deviation 1.4301	Average 1.4571	Sd. Deviation 1.4571
Fm	[kN]	24.59	0.80	19.03	0.342
σ_u	[MPa]	725.8	27.69	658.7	25.12
$\sigma_{p0.2}$	[MPa]	417.2	21.65	377.0	13.78
ε_c	[%]	0.387	0.008	0.353	0.022
$\sigma_{p0.01}$	[MPa]	265.7	13.08	183.7	29.62
$\sigma_{p0.05}$	[MPa]	334.2	10.71	291.9	10.17
$\sigma_{p1.0}$	[MPa]	471.1	25.01	430.9	17.62
$\varepsilon_{1.0}$	[%]	1.21	0.005	1.20	0.007
$\sigma_{2.0}$	[MPa]	487.3	25.44	445.2	18.11
ε_u	[%]	45.49	0.686	44.69	0.482
$k_{2\%}$ [4] (calculated)	[-]	0.227	0.015	0.245	0.005
$k_{2\%}$ [14] (calculated)	[-]	1.168	0.001	1.181	0.011
E_a	[GPa]	221.57	4.41	211.91	9.18
n [17] (calculated)	[-]	6.64	-	4.17	-
m [17] (calculated)	[-]	3.01	-	3.00	-

exposed to the high temperature. At higher temperatures, the colours are usually reported as grey or dark grey as thicker oxides are developed. As the time at elevated temperature increases, the colours change from yellow to red and then to blue. This is expected because the oxide becomes thicker over time [18].

3. Simplified calculation methods

The simplified method proposed in [1], is used to predict the load-displacement behaviour (which is only valid for small displacements). Deflections may be determined considering the non-linear constitutive law of stainless steel, being estimated using the secant and tangent modulus. For any load level, the maximum bending moment M_{max} is determined. For the case of the 3-point bending setup, the Eq. (1) is used to determine the stress at the extreme fibre σ.

$$\sigma = k_\sigma \frac{M_{max}}{W_e} \tag{1}$$

The factor k_σ is introduced to avoid very large deflections due to the calculation procedure to find the average secant modulus E_S at the section for the maximum bending moment and also due to the calculation of the stress in the extreme fibres. This factor should be lower or equal to the unity ($k_\sigma = 0.8$). The W_e represents the elastic section modulus of the cross-section. The equivalent modulus E_{eq} is based on the average value obtained from the secant E_S and tangent E_T modulus, see Eq. (2) - Eq (3).

$$E_{eq} = (E_S + E_T)/2 \tag{2}$$

$$E_S = \left[1 + 0.002 \frac{E_0}{\sigma_{0.2}} . \left(\frac{\sigma}{\sigma_{0.2}}\right)^{n-1}\right]^{-1}, E_T$$
$$= \left[1 + 0.002.n. \frac{E_0}{\sigma_{0.2}} . \left(\frac{\sigma}{\sigma_{0.2}}\right)^{n-1}\right]^{-1} \times E_0 \tag{3}$$

Where E_0 represents the initial elastic modulus, $\sigma_{0.2}$ the proportional stress at 0.2% strain, σ the stress used for the modulus calculation and n is a constant determined by requiring that the modified Ramberg-Osgood curve intersected the measured stress-strain curve for the proportional stress at 0.05%. These values are based on the tension and compression values for the extreme fibres at the cross-section of the maximum bending moment (central zone of the beam), following the constitutive law of Ramberg-Osgood. They were determined for each

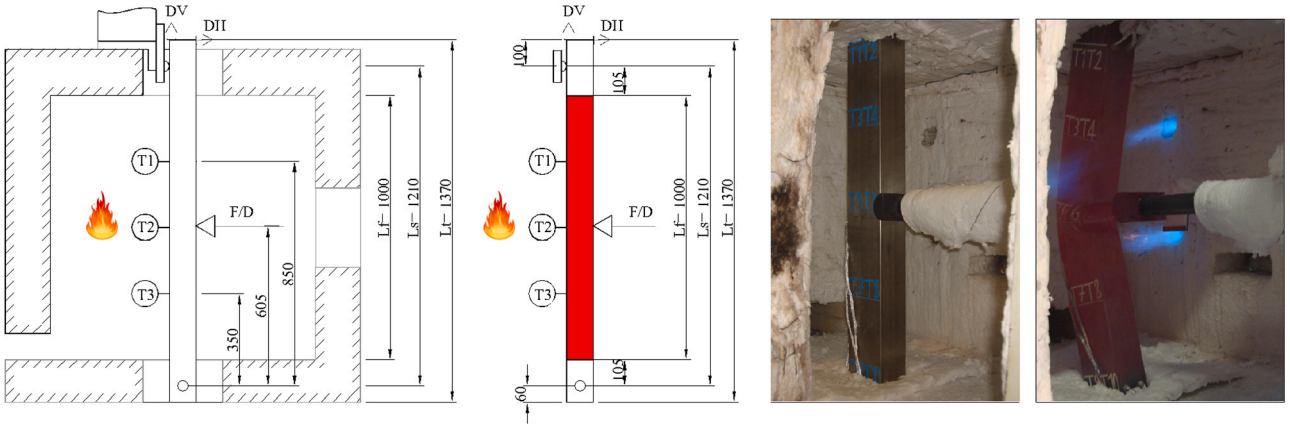

Fig. 3. Experimental setup with stainless steel beam (Specimen 3) before and after the test.

Table 2
Specimens under bending test at elevated temperature (Temp.).

Specimens	Test number	Material grade	Temp. [°C]	Maximum load EXP [kN]	Maximum load NUM [kN]	Relative Difference [%]	Maximum load NUM CORNER [KN]	Relative difference CORNER [%]
1	EXP 1	1.4301	500	51.63	48.27	-5.38	57.51	+ 12.73
2	EXP 2	1.4301	500	50.40				
3	EXP 1	1.4301	700	38.10	36.79	-5.02	41.26	+ 10.46
4	EXP 2	1.4301	700	37.26				
5	EXP 1	1.4571	500	49.10	55.73	+ 13.50	66.84	+ 36.12
6	EXP 2	1.4571	500	49.11				
7	EXP 1	1.4571	700	39.23	46.46	+ 18.32	53.96	+ 37.43
8	EXP 2	1.4571	700	39.30				

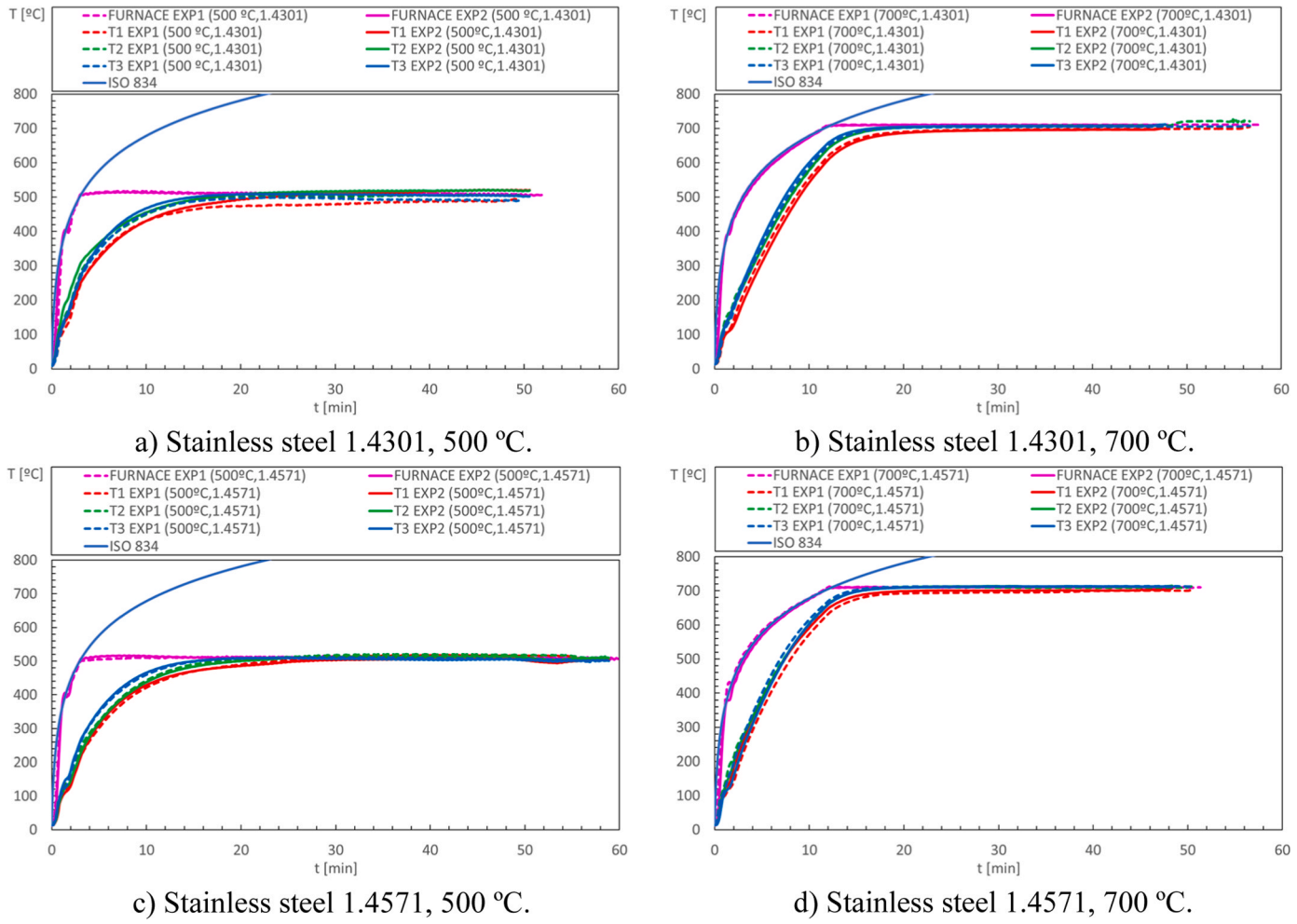

Fig. 4. Heating the beams to steady conditions.

temperature level, based on the values of the experimental tensile tests. The constant value of 3.56 is used for the parameter n [1]. The maximum deflection is then calculated according to Eq. (4), replacing the Elastic modulus E_0, with the equivalent elastic modulus E_{eq}.

$$D = \frac{PL^3}{48E_{eq}I} \tag{4}$$

A similar approximation is presented by the current version of EN 1993–1–4 [17], using only the secant modulus of elasticity, as an average between the value determined for the compression and tension flanges. The values for the secant modulus may be estimated by Eq. (5), where $\sigma_{i.Ed,ser}$ represents the serviceability design stress, f_y the yield strength, and n depends on the grade of the stainless steel ($n = 6$).

$$E_S = E_0 \Big/ \left[1 + 0.002\frac{E_0}{\sigma_{i.Ed,ser}}\left(\frac{\sigma_{i.Ed,ser}}{f_y}\right)^n\right] \tag{5}$$

4. Numerical model

The numerical model is based on the finite element method using the Ansys Parametric Design Language (APDL). The average surface of the SHS150×100×3 section is modelled using the SHELL181 finite element, with four nodes with six degrees of freedom at each node, displacements and rotations along the X, Y and Z axes, suitable for the analysis of thin to moderately thick shells, in the linear and non-linear regime of large deformations, including the plastic behaviour of the material. This element uses linear interpolating functions, and full integration with incompatible modes to enhance the accuracy in bending-dominated problems. Rigid beam finite elements have been used to simulate the loading device, using BEAM188 finite element, with 3 nodes with six degrees of freedom at each node (the same used for the shell). This element used linear interpolating functions, and one integration point along the length. The finite element model is presented in Fig. 8. The beam is subjected to a 3-point bending setup, considering bi-articulated support (at the bottom support) and simple support with restraint to the normal direction from all nodes of the lower flange of the section (at the top support). The beam presents a total length of $L_t = 1.37$ [m], a bending length of $L_s = 1.21$ [m] and a heat-affected length is $L_f = 1.0$ [m]. The number of shell finite elements is 6624 and the number of beam finite elements is 42, both used over 6716 nodes. The shell finite element size changes from $6 \times 16\ mm^2$ in the flat region to $1.17 \times 16\ mm^2$ in the corner regions, to get a better approximation of the real deformation shape obtained from the experimental test. The bending load is distributed over the nodes (nodal forces) where the beam finite elements are attached. This boundary condition is used to mimic the solid extension rod from the test setup, see Fig. 3.

The material model is the same for all the regions of the beam. Residual stresses were not included in simulations, since their effect was considered very small at elevated temperatures, as proved by Lopes et al. in 2010 [7]. The constitutive law was defined for all the temperature levels, using the true stress-true strain curves, see Fig. 9. At elevated temperatures, these curves were determined based on the reduction factors given by the [14]. An alternative material model was developed to accommodate the effect of the manufacturing RHS process (cold

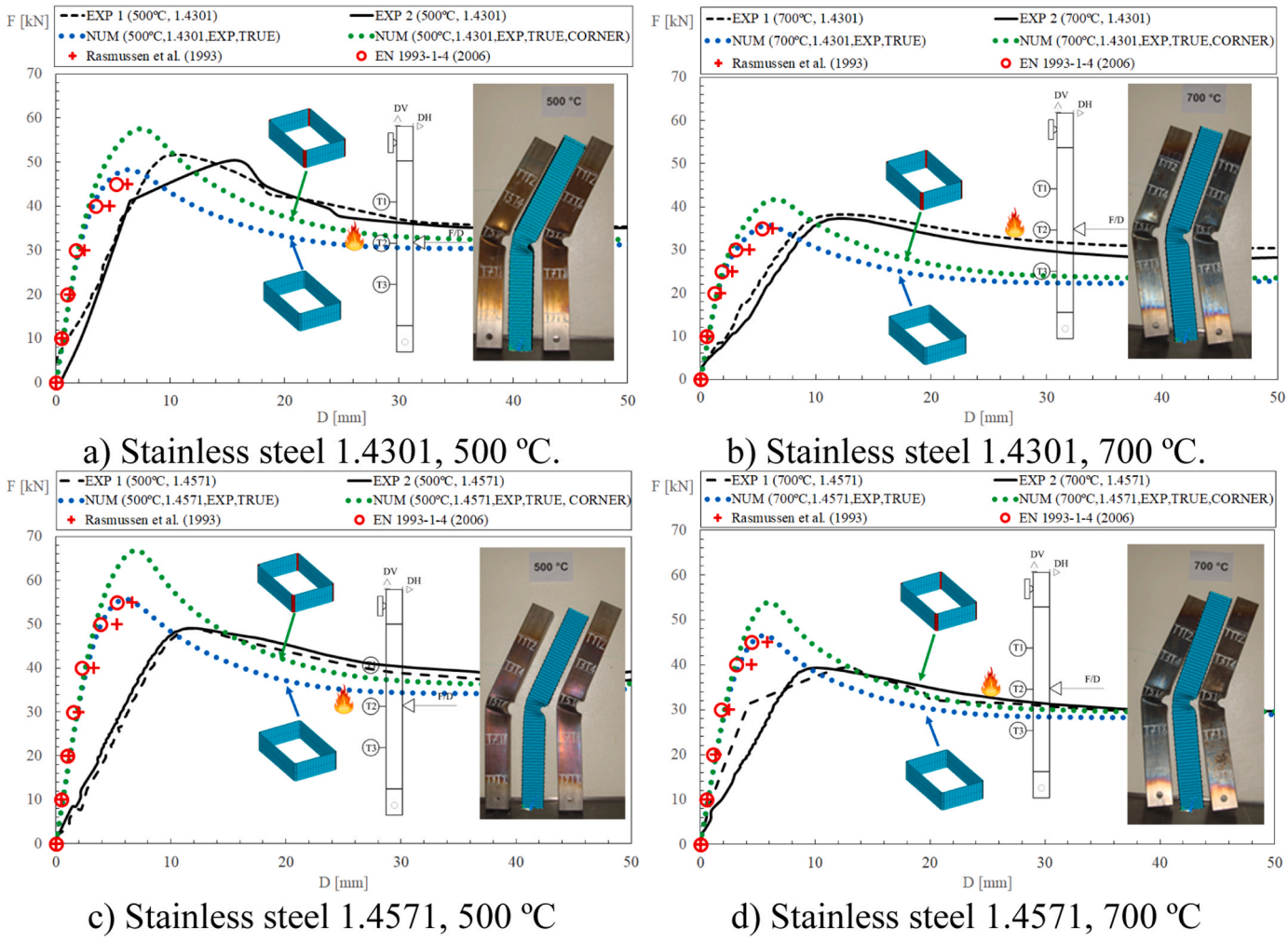

Fig. 5. Bending resistance at elevated temperature (load-displacement).

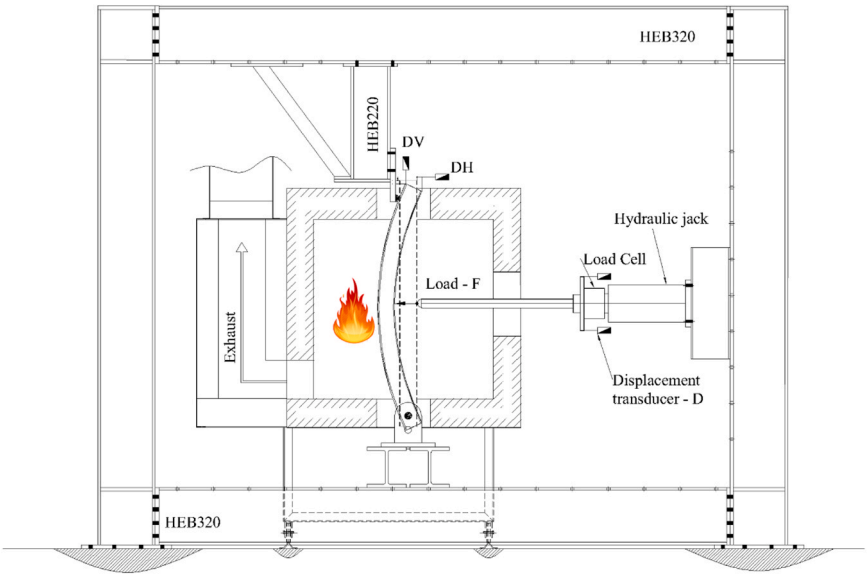

Fig. 6. Predicted deformed shape of the beams on the test setup.

forming). This effect is responsible for increasing the yield stress $\sigma_{p0.2,c}$ and the ultimate stress $\sigma_{u,c}$ in the corner regions. The true stress true strain curves are also based on the Ramberg Osgood constitutive model just by modifying the yield stress and ultimate stress, using Eq. (6) and Eq. (7), respectively and presented by Ashraf et al. [19].

Fig. 7. Deformed shape mode for all the specimens.

$$\sigma_{p0.2,c} = \frac{1.881\sigma_{p0.2}}{(r_i/t)^{0.194}} \tag{6}$$

$$\sigma_{u,c} = 0.75\sigma_{p0.2,c} \quad (\sigma_u/\sigma_{p0.2}) \tag{7}$$

Eq. (6) is independent of the ratio between the ultimate and yield strength $\sigma_u/\sigma_{p0.2}$. It only depends on the internal corner radius $r_i = 3mm$ and thickness $t = 3mm$ of the RHS section. For the prediction of the ultimate strength in the corner region $\sigma_{u,c}$, Eq. (7) was considered, assuming a dependence on the ratio between the ultimate and yield strength of the virgin material and also on the yield just determined to the corner region [19]. Fig. 9 presents the difference between the material model used for the flat zone and those used for the corner regions. There is a big reduction in ductility and a big increase in strength for both stainless steel grades.

The number of vector forces applied to the loading zone is also responsible for modifying the load-displacement curve. If one changes the number of nodal force vectors from 45 to 57, just by applying 12 extra nodal forces in the corner nodes of the flange, the load-bearing increases by 5 [kN], for the case of the stainless steel grade 1.4301. This means that the loading system and the interaction with the beam specimen (region affected by the load) are also responsible for modifying the load-displacement curve, and this contact zone changes during the experimental tests.

4.1. Validation of the model

The GMNIA models consider the two-stage Ramberg Osgood constitutive material law, based on material properties experimentally determined at room temperature. The reduction coefficients from the second generation of EN1993–1–2 were used to define the mechanical behaviour at elevated temperatures [14]. The engineering curves were modified to true stress and true strain material models. As local buckling phenomena were likely to occur, shell finite elements were defined with an initial concavity and convexity for both sides of the hollow section corresponding to 80% of the essential manufacturing tolerances as proposed in EN1993–1–5 [20] (± 0.5 mm), defined by EN 10219–2 [21]. These imperfections are based on the first mode of local buckling instability determined by linear elastic analysis and are an alternative method to the geometric imperfection measurements as presented in Xing et al. [22]. The nominal dimensions from the stainless steel structural element RHS 150×100×3 were used, because there was a small difference concerning the measured dimensions (positive difference of 0.275% on average) with no significant impact on the load-displacement

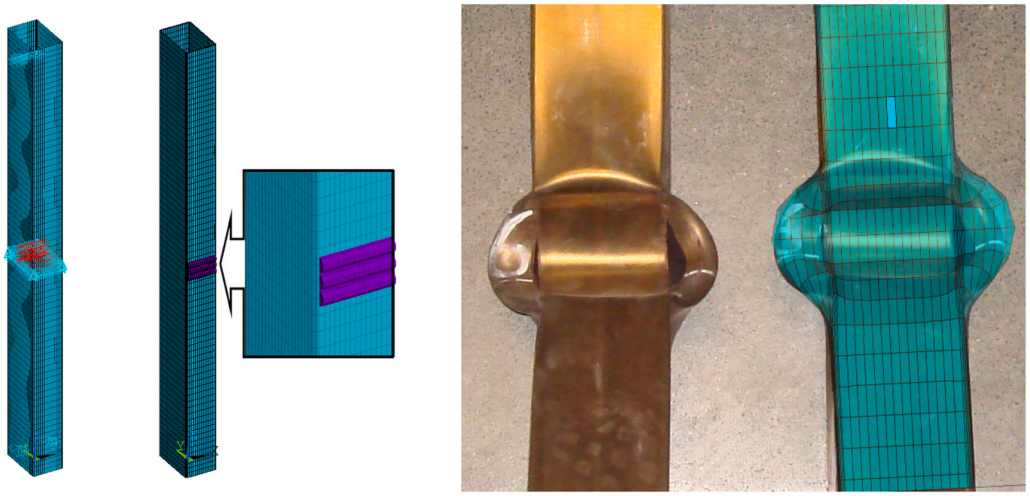

Fig. 8. – Finite element model and comparison of the deformed shape from specimens 1 and 2.

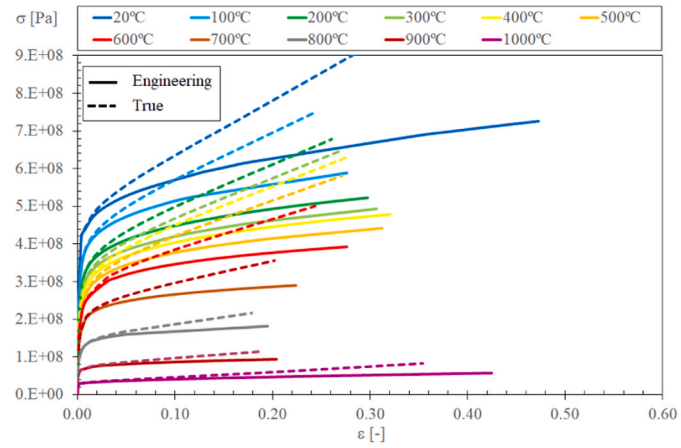

a) Stainless steel grade 1.4301, without strain hardening effect.

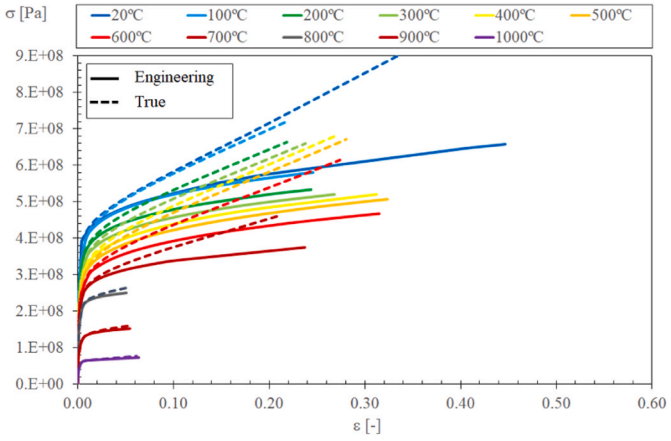

b) Stainless steel grade 1.4571, without strain hardening effect.

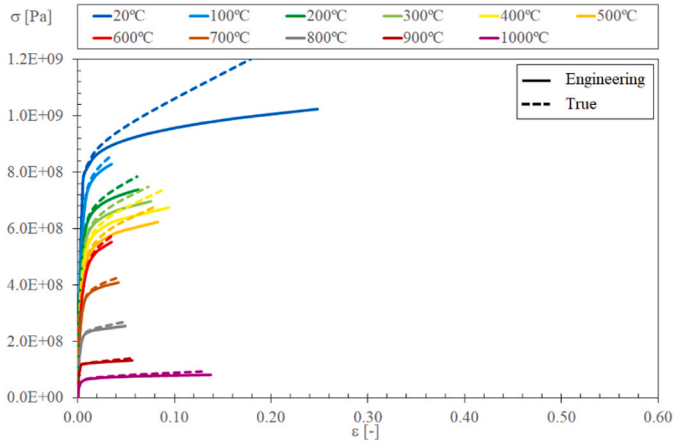

c) Stainless steel grade 1.4301, with strain hardening effect in the corner region.

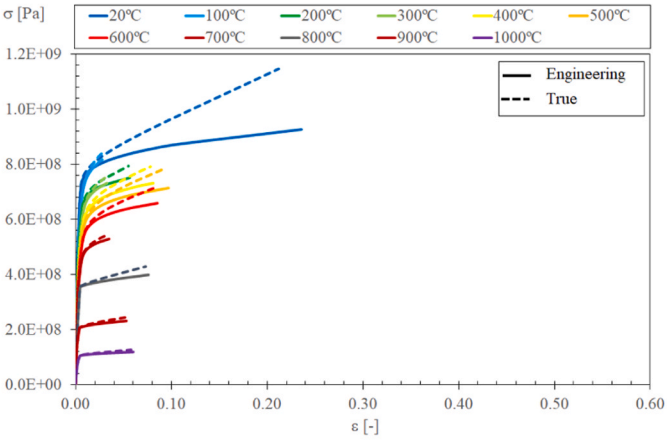

d) Stainless steel grade 1.4571, with strain hardening effect in the corner region.

Fig. 9. Stress-strain for both steel grades at elevated temperatures (engineering stress-strain model from [17]).

curve and bending resistance. The solution method includes an incremental force based on the arc-length method (variable load from 0.05 N to 5000 N). The convergence criterion is based on displacement, using a tolerance value of 0.1% and a reference value of 0.1 m. The numerical results agree very well with the experimental results, see Fig. 5, and the model can predict the post-buckling behaviour, just by restraining the vertical displacement of the central nodes of the beam (important to model the post buckling). The deformed shape mode is also in agreement with the experimental results, see Fig. 8. The numerical model does not include the material damage. This damage effect is due to the loss of the material ductility during the processing conditions to obtain the stainless steel profile (direct forming). This processing condition is responsible for reducing ductility and increasing the yield strength of the corner regions when compared to the flat regions. These types of structural elements exhibit poor plastic deformation capacity, as mentioned by Landolfo [16] and observed during the experimental tests. Both material models (without and with the corner effect) were evaluated. The corner effect is responsible for increasing the bending resistance of the numerical models by an average value of 19% at 500 ºC and 16% at 700 ºC. The experimental bending resistance of the steel grade 1.4301 is between these two numerical model results. The experimental bending resistance from grade 1.4571 is over-predicted by both material models, see Table 2.

The bending resistance (maximum load) is well predicted by the finite element model for the case of the stainless steel grade 1.4301 with a relative difference of − 5.38% at 500 ºC and − 5.02% at 700ºC, when considering the same material model for the flat and corner regions. The difference increases to + 12.73% and + 10.46% when considering two different material models for both regions (flat and corner). The numerical model over-predicts the bending resistance for grade 1.4571, with a relative difference of + 13.50% at 500ºC and + 18.32% at 700 ºC when assuming the same material model for both regions. The difference increases to + 36.12% at 500 ºC and + 37.43% at 700 ºC, when considering two distinct material models. This may suggest that the reduction coefficients proposed to grade 1.4571 do not mimic the real material behaviour at 700 ºC. If one compares the reduction factors from both grades one can conclude that $k_{p0.2,\Theta}$ is 55% higher at this temperature level, $k_{u,\Theta}$ is 42% higher, $k_{2,\Theta}$ is 44% higher, when compared to grade 1.4301. The relation between the flat and the corner zones for the 0.2% proof strength and the ultimate strength presented in Ashraf et al. [19] also presents a certain degree of dispersion, even if the coefficient of determination is close to unity, contributing to increasing the over-prediction of bending resistance. The bending resistance decreases with temperature, as expected. The difference in the initial stiffness response

is related to the setup configuration of the test rig. The initial slops determined by the numerical model are different from the experimental results. This is usually due to the initial slack behaviour of the specimen caused by the assembling tolerance (gaps and loose contact) and due to the vertical extension used in the reaction frame (support). Nevertheless, the model agreement in the nonlinear features of the load-displacement curve was acceptable and thus the model was considered applicable for the subsequent bending resistance, because the load bearing and the post-buckling deformed mode shape are well predicted.

4.2. Parametric analysis

The parametric study is focused on the cross-section type, temperature level and material grade, see Table 3. Based on the nominal dimensions and properties, all the cross-sections are classified as slender, considering the calculation of the relative slenderness at elevated temperature, according to the second generation of EN1993–1–2 [14]. The material strength at elevated temperature should be considered at 2% total strain, $f_{2,\theta}$, for all cross-section classes. The effective section modulus for slenderness sections, W_{eff}, was determined based on the second order moment of the effective area. Based on the validation model, one single material was considered for the flat and corner regions.

Sixty-six simulations were developed to determine the bending resistance at elevated temperatures. The numerical results are, in most of the cases, underpredicting the elastic load F_{el}, the plastic load F_{pl} and the effective load F_{eff}, see Fig. 10 to Fig. 12.

The stainless steel beam cross-section SHS (3) has numerical results in close agreement with the calculation of the effective resistance for all the temperature levels, including room temperature if one considers the reduction coefficient $k_{2,\theta}$ at room temperature determined by experiments (1.16 and 1.18, for grade 1.4301 and 1.4571 respectively). The relative difference for the load bearing, when comparing the numerical with the analytical results, changes between + 4.7% at 1000ºC and + 0.1% at room temperature for grade 1.4301, while these values change to − 3.7% at 1000 ºC and − 0.8% at room temperature for grade 1.4571, see Fig. 10.

The stainless steel beam cross-section RHS (3) has also numerical results in good agreement with the calculation of the effective resistance. The relative difference changes between − 2.6% at elevated 1000ºC and − 13.1% at room temperature for grade 1.4301, while these values change to − 19.4% at 1000 ºC and − 13.0% at room temperature for grade 1.4571, see Fig. 11.

The stainless steel beam cross-section RHS (6) has also numerical results in close agreement with the calculation of the effective resistance. The relative difference changes between + 5,4% at elevated 1000ºC and − 1.2% at room temperature for grade 1.4301, while these values change to − 9,5% at 1000 ºC and − 1.6% at room temperature for grade 1.4571, see Fig. 12.

These results confirm that the Eurocode design rules for slender cross-sections are, in general, safe for all temperature levels, being able to predict the bending resistance of beams. The slender cross-section, RHS (3) presents a higher difference between the numerical results and the analytical prediction, which may be related to the material model used for thinner elements. The bending resistance for normal temperature conditions appears to be unsafe if one considers the reduction coefficient $k_{2,\theta} = 1.31$.

Table 3
Parametric study.

Material grade	Cross sections	Temperature level [ºC]
1.4301 1.4571	RHS 150×100×3 (RHS 3), RHS 150×100×6 (RHS 6), SHS 100×100×3 (SHS 3)	20, 100, 200, 300, 400, 500, 600, 700, 800, 900, 1000

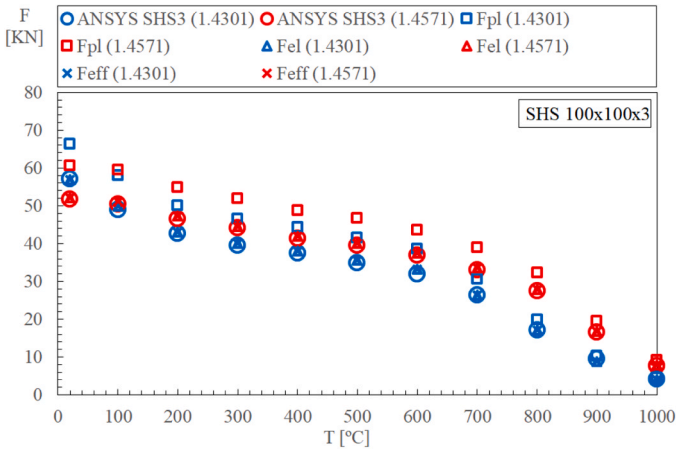

Fig. 10. Bending resistance of stainless steel hollow SHS 100×100×3.

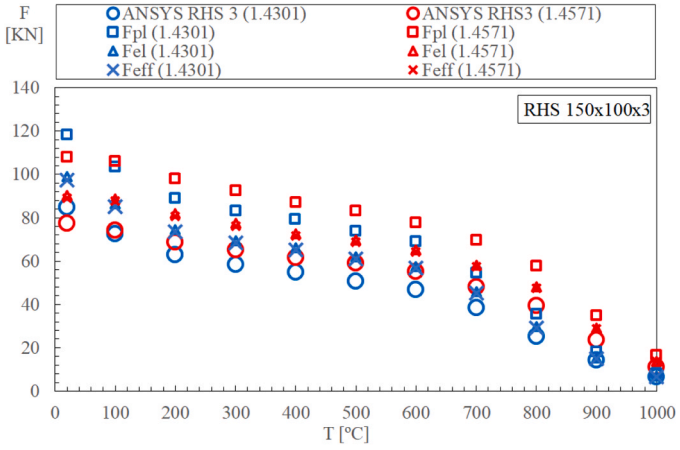

Fig. 11. Bending resistance of stainless steel hollow RHS 150×100×3.

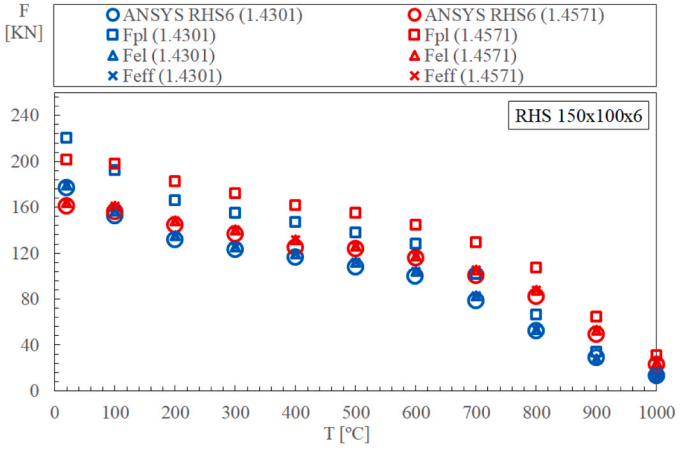

Fig. 12. Bending resistance of stainless steel hollow RHS 150×100×6.

5. Conclusions

Eight experimental fire resistance tests to stainless steel beams were presented and it was possible to observe and record the load-

displacement behaviour of the beams at high temperatures. The experimental test setup made it possible to mobilize a load close to the maximum resistance of the cross-section. It was possible to verify significant hardening of stainless steel at high temperatures. Stainless steel grade 1.4751 presents higher bending resistance at high temperatures when compared to grade 1.4301, especially due to the effect of the reduction coefficients.

A 3D numerical model was validated for each material grade at 500 and 700 ºC, using eight experimental tests. The numerical simulations for stainless-steel grade 1.4301 presented the most accurate results with a relative difference of − 5.38% at 500 ºC and − 5.02% at 700ºC, which means that the numerical model underpredicts the experimental results. This relative difference increased for the steel grade 1.4571, reaching + 13.51% and + 18.32% for both temperature levels, 500 and 700 ºC respectively, which means that the numerical results are overpredicting the experimental results. The strain hardening effect in the corner regions was also investigated, revealing an increase in the bending resistance by an amount of 19% at 500ºC and 16% at 700ºC, both overprediting the bending resistance determined by the experimental results. In these cases, the difference between the numerical and experimental results attained + 12.7% and + 10.46 for grade 1.4301%, and 36.1% and 37.43% for grade 1.4571, at 500ºC and 700ºC respectively. According to Ashraf et al. [19] the coefficient of determination for the 0.2% proof strength, relating both zones (corner and flat) is close to 1 but one can see some scattered data points that can explain this over-prediction in the bending resistance. This is something that deserves investigation in parallel with testing the material in corner regions at elevated temperatures.

The finite element model has been used to determine the effect of the cross-section and the effect of the temperature level. The bending resistance determined with ANSYS is in close agreement with the design moment resistance (effective cross-section) for the less slender cross sections (SHS (3) and RHS (6)). The reduction coefficients $k_{2,\theta}$, used for the calculation of the design moment resistance, seem to be working properly for each material grade and temperature level, except for 20 ºC. The reduction coefficient proposed by the future generation of the EN1993–1–2, for both material grades is 1.31, but from the tensile tests, one determined 1.16 for grade 1.4301 and 1. 18 for grade 1.4571. This difference should be related to the flat region where coupons were extracted from, but more tensile tests should be developed. The material grade 1.4571 has higher bending resistance at elevated temperatures than grade 1.4301, but smaller bending resistance at room temperature.

Declaration of Competing Interest

The authors declare that they have no known competing financial interests or personal relationships that could have appeared to influence the work reported in this paper.

References

[1] Rasmussen KJR, Hancock e GJ. Design of cold-formed stainless steel tubular members. II: Beams (Ago) J Struct Eng 1993;vol. 119(n. 8):2368–86. https://doi.org/10.1061/(ASCE)0733-9445(1993)119:8(2368).

[2] Gardner L, Baddoo e NR. Fire testing and design of stainless steel structures. J Constr Steel Res . 2006;vol. 62(n. 6):532–43. https://doi.org/10.1016/j.jcsr.2005.09.009.

[3] The Steel Construction Institute, Design Manual For Structural Stainless Steel, 3rd ed., n. April. The Steel Construction Institute, 2006.

[4] CEN, "EN1993–1.2: 2005 - Eurocode 3: Design of steel structures - Part 1–2: General rules - Structural fire design", *CEN- European Committee for Standardization*. Brussels, 2005.

[5] Gardner L, Ng e KT. Temperature development in structural stainless steel sections exposed to fire. Fire Saf J 2006;vol. 41(n. 3):185–203. https://doi.org/10.1016/j.firesaf.2005.11.009.

[6] Ng KT, Gardner e L. Buckling of stainless steel columns and beams in fire. Eng Struct 2007;vol. 29(n. 5):717–30. https://doi.org/10.1016/j.engstruct.2006.06.014.

[7] Lopes N, Real PV, da Silva LS, Franssen e JM. Numerical modelling of thin-walled stainless steel structural elements in case of fire. Fire Technol 2010;vol. 46(n. 1):91–108. https://doi.org/10.1007/s10694-009-0084-x.

[8] Huang Y, Young e B. Structural performance of cold-formed lean duplex stainless steel beams at elevated temperatures. Thin-Walled Struct 2018;vol. 129(n. February):20–7. https://doi.org/10.1016/j.tws.2018.03.031.

[9] Z. Xing, O. Zhao, M. Kucukler, e L. Gardner, "Fire testing and design of slender stainless steel I-sections in weak-axis flexure", *Thin-Walled Structures*, vol. 171, n. August 2021, p. 108682, Fev. 2022, doi: https://doi.org/10.1016/j.tws.2021.108682.

[10] Lopes N, Arrais F, Vila Real P, Alves M, Mesquita L, Piloto P, et al. Fire resistance of austenitic stainless steel beams with rectangular hollow sections. Fire Mater . 2023:1–14. https://doi.org/10.1002/fam.3167.

[11] Xing Z, Kucukler M, Gardner e L. Local buckling of stainless steel I-sections in fire: Finite element modelling and design (p) Thin-Walled Struct 2021;vol. 161(n. January):107486. https://doi.org/10.1016/j.tws.2021.107486.

[12] Vila Real PMM, Lopes N, Simões da Silva L, Franssen e JM. Lateral-torsional buckling of stainless steel I-beams in case of fire. J Constr Steel Res 2008;vol. 64(n. 11):1302–9. https://doi.org/10.1016/j.jcsr.2008.04.013.

[13] Xing Z, Zhao O, Kucukler M, Gardner e L. Testing of stainless steel I-section columns in fire. Jan. 2021 Eng Struct 2020;vol. 227(n. November):111320. https://doi.org/10.1016/j.engstruct.2020.111320.

[14] FprEN CEN. -2:2023 - Eurocode 3 - Design of steel structures - Part 1-2: Structural fire design Eurocode", *CEN- European Committee for. Stand* CEN- Eur Comm Stand 1993-1:2023.

[15] ISO, "ISO 6892–1: Metallic materials — Tensile testing — Part 1: Method of test at room temperature", *International Organization for Standardization*. ISO, Geneve, 2009.

[16] Landolfo R. Material ductility and buckling behaviour of eurocode-compliant cold-formed steel hollow columns (Set) ce/Pap 2022;vol. 5(n. 4):1–8. https://doi.org/10.1002/cepa.1721.

[17] CEN, "EN 1993–1-4:2006 - Eurocode 3: Design of steel structures - Part 1–4: General rules - Supplementary rules for stainless steels", *CEN- European Committee for Standardization*. CEN, Brussels, 2005.

[18] Higginson RL, Jackson CP, Murrell EL, Exworthy PAZ, Mortimer RJ, Worrall DR, et al. Effect of thermally grown oxides on colour development of stainless steel. Mater High Temp 2015;vol. 32(n. 1–2):113–7. https://doi.org/10.1179/0960340914Z.00000000083.

[19] Ashraf M, Gardner L, Nethercot e DA. Strength enhancement of the corner regions of stainless steel cross-sections. J Constr Steel Res . 2005;vol. 61(n. 1):37–52. https://doi.org/10.1016/j.jcsr.2004.06.001.

[20] CEN, EN. *1993-1-5: Eurocode 3 — Design of steel structures — Part 1-5: Plated structural elements*, CEN-Europ. Brussels: CEN- European Committee for Standardization 2006.

[21] CEN, "EN10219–2: Cold formed welded structural hollow sections of non-alloy and fine grain steels - Part 2: Tolerances, dimensions and sectional properties". CEN - European Committee for Standardization, Brussels, 2006.

[22] Xing Z, Jiang M, San B, Wu e K. Experimental investigation of austenitic stainless steel I-section stub columns at elevated temperatures. 2022, p Thin-Walled Struct . 2023;vol. 184(n. December):110502. https://doi.org/10.1016/j.tws.2022.110502.